Electronic Supplementary Material (ESI) for Nanoscale.
This journal is © The Royal Society of Chemistry 2022

Supporting Information

Contents

17. *Figure S16* – log(i) vs log(υ) plot at different voltages for 2-electrode system and deconvoluted current contributions at different scan rates

18. *Figure S17* – Gradual change in transmission spectra of the multicolored device upon application of bias

19. *Figure S18* – Cycling performance of MECASC and GCD profiles with dynamic in-situ

    transmission modulations before and after cycling

20. *Figure S19* – Morphology of V_2O_5 electrode before and after cycling

21. *Figure S20* – Morphology of PANI electrode before and after cycling

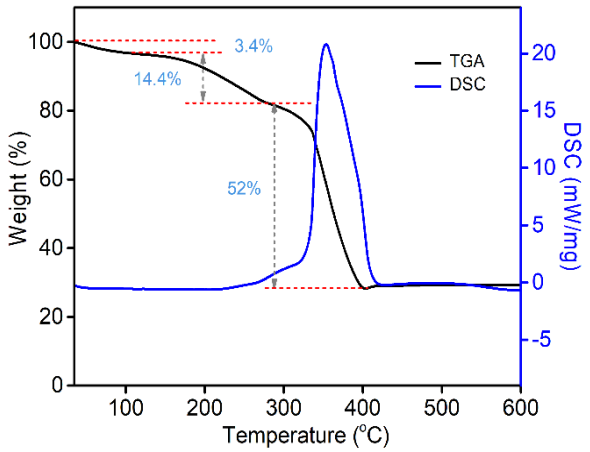

Figure S1: TGA and DSC data for V-MOF

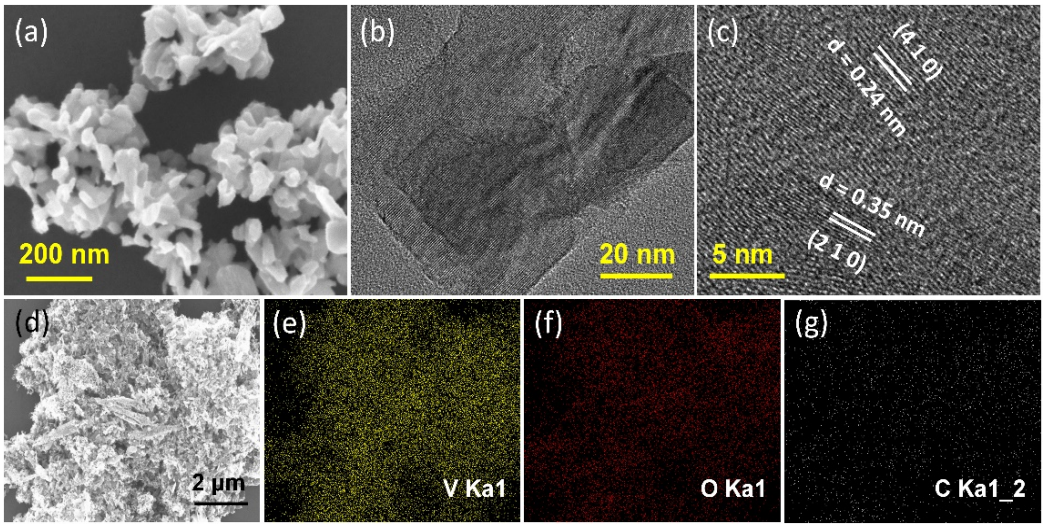

Figure S2: SEM, TEM and EDX mapping data for V_2O_5-2 sample

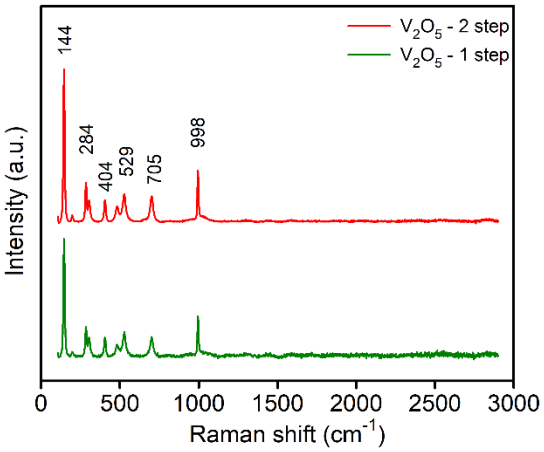

Figure S3: Raman data for both V_2O_5 samples

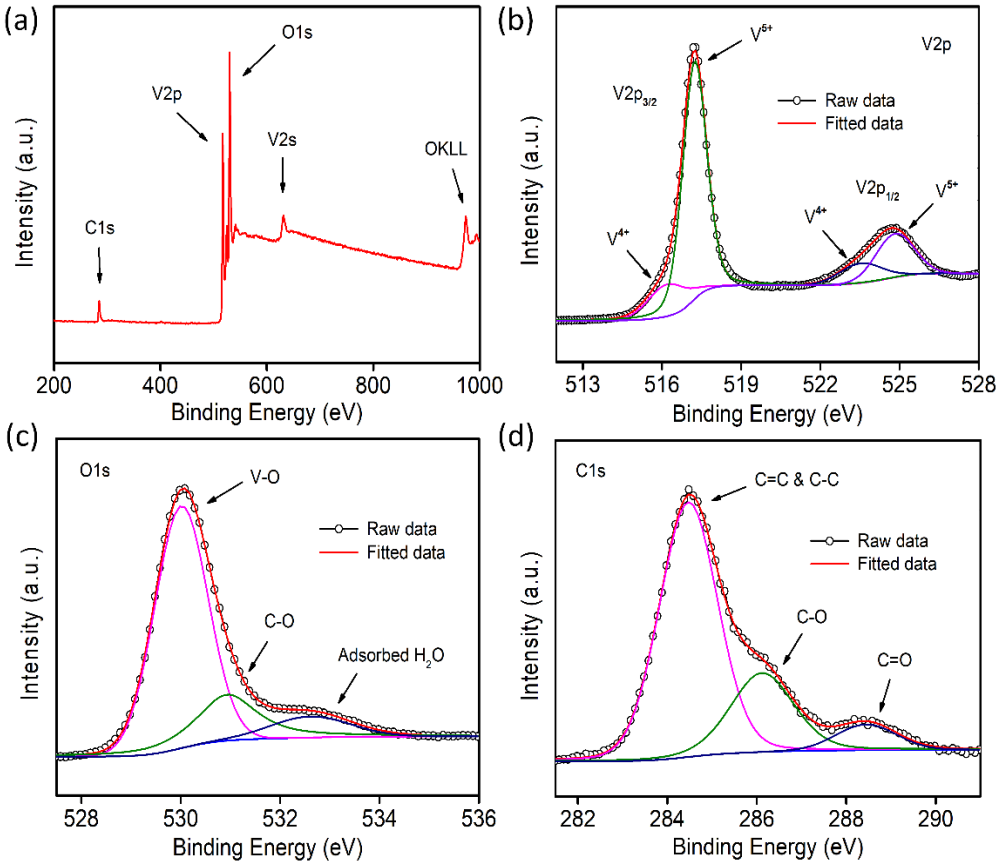

Figure S4: XPS data including survey spectra and the deconvoluted spectra of V_2O_5-2 sample

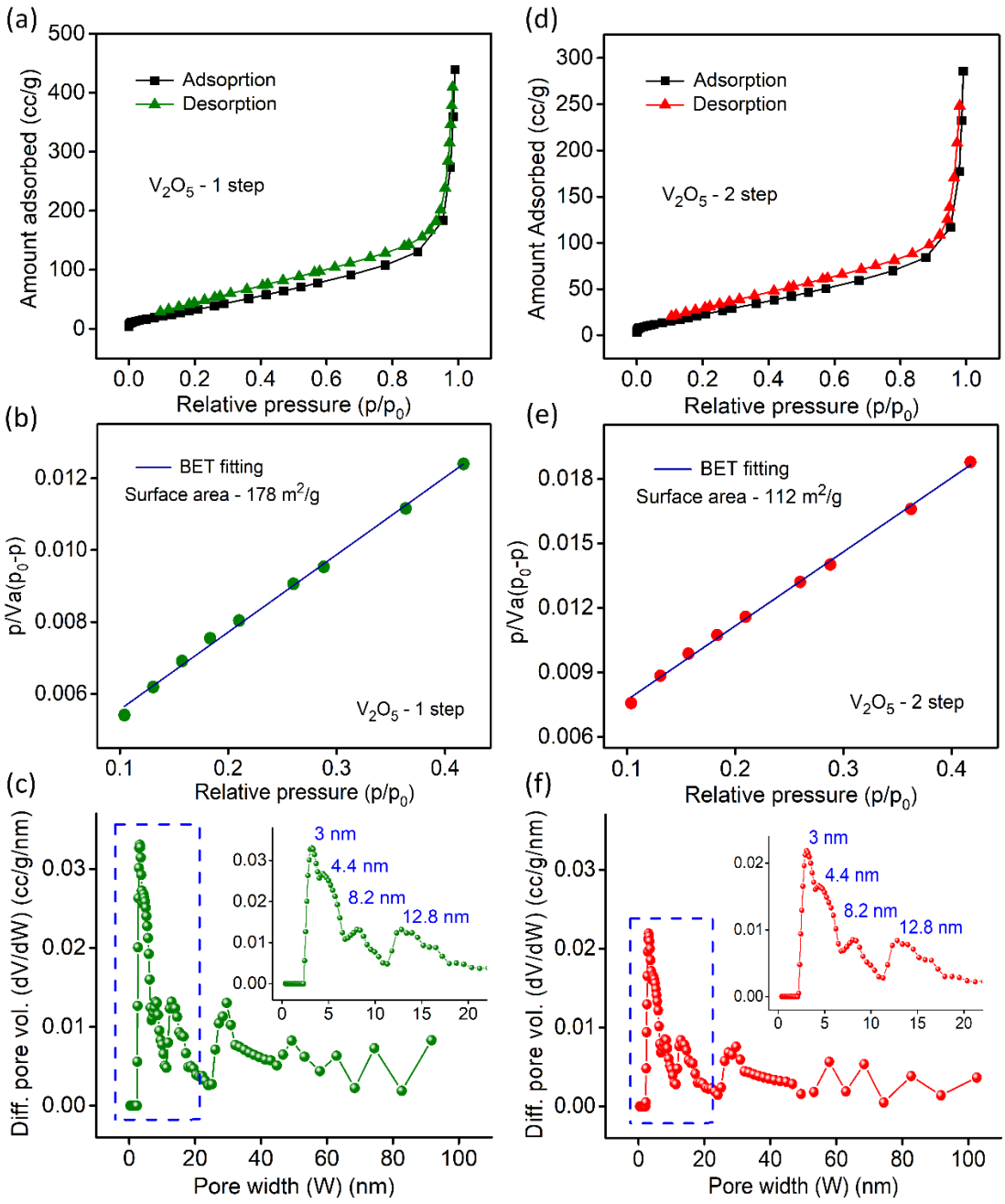

Figure S5: N_2 gas adsorption isotherm at 77 K, BET fitting data and NLDFT pore size distribution data for (a)-(c) V_2O_5-2 and (d)-(f) V_2O_5-1 samples

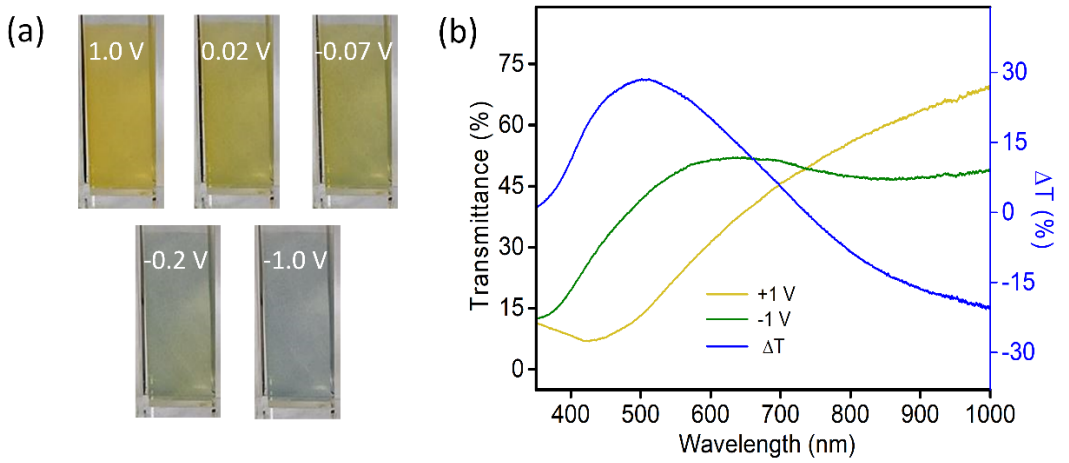

Figure S6: (a) Photographs of V_2O_5-1 electrode at different potentials, (b) Transmission and optical modulation spectra of V_2O_5-2 electrode in 3-electrode set-up

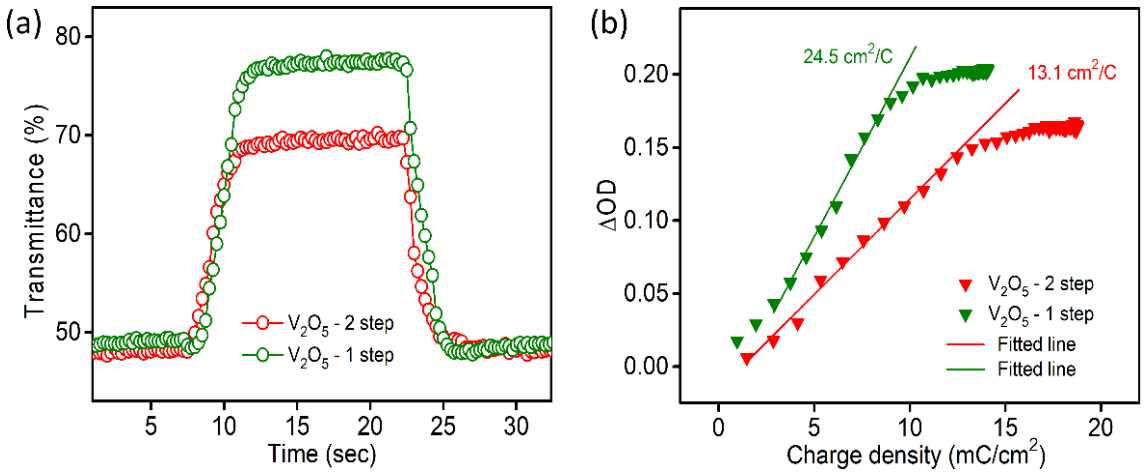

Figure S7: (a) Switching times and (b) coloration efficiencies at 1000 nm for both samples

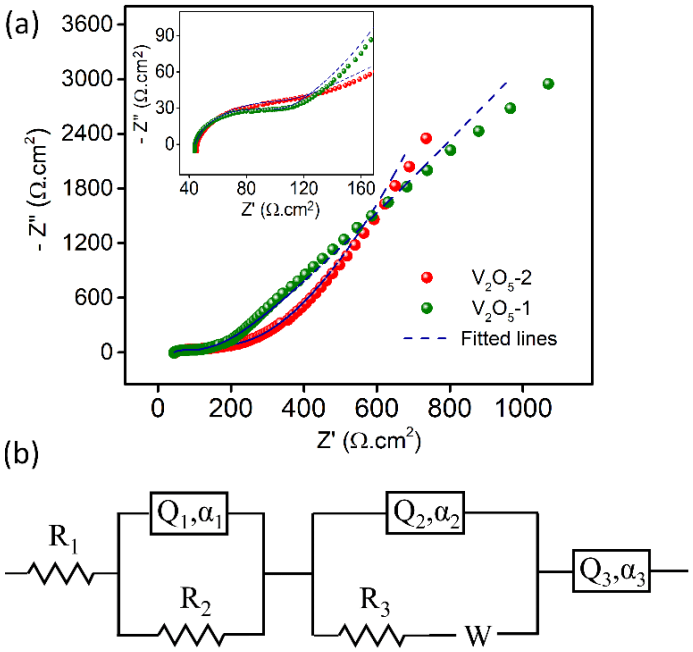

Figure S8: (a) Nyquist plots of the samples, (b) equivalent circuit diagram

Table S1: Comparison of resistance values obtained from modelling the Nyquist plots

Films	R_1 (Ωcm^2)	R_2 (Ωcm^2)	R_3 (Ωcm^2)	Measurement error (%)
V_2O_5-1	43.87	50.2	58.1	< 3.31
V_2O_5-2	45.31	97.1	60.3	< 2.95

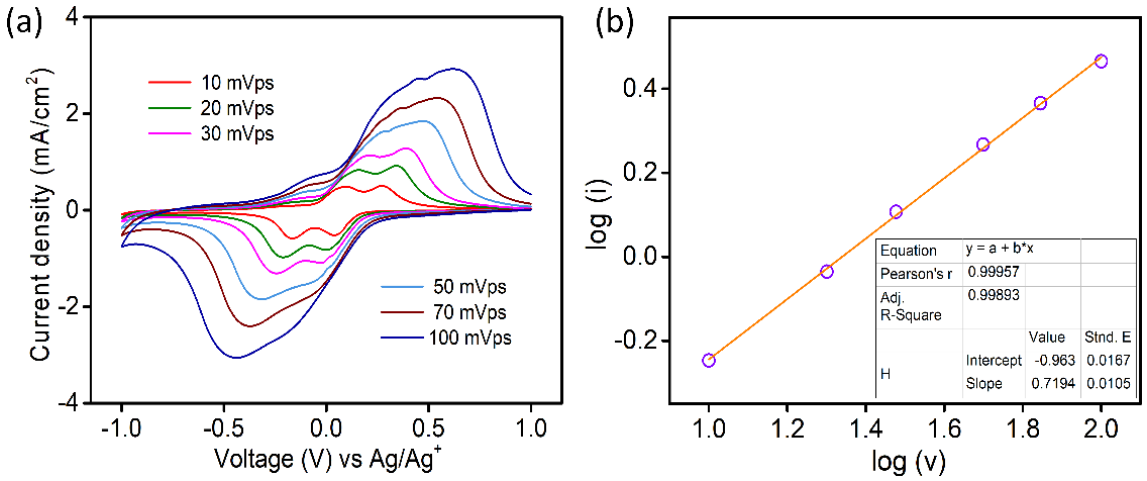

Figure S9: (a) Scan rate dependent CV data and (b) log(i) vs log(υ) plots for V_2O_5-2 electrode

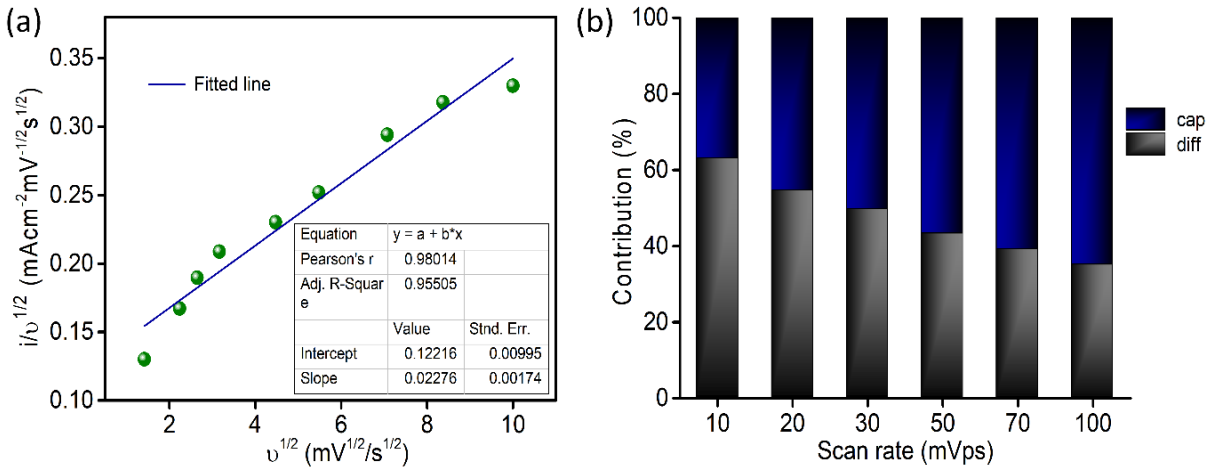

Figure S10: (a) $i/\upsilon^{1/2}$ vs $\upsilon^{1/2}$ plot for V_2O_5-1 electrode and (d) histogram plot shows the decoupling of current contributions with scan rate

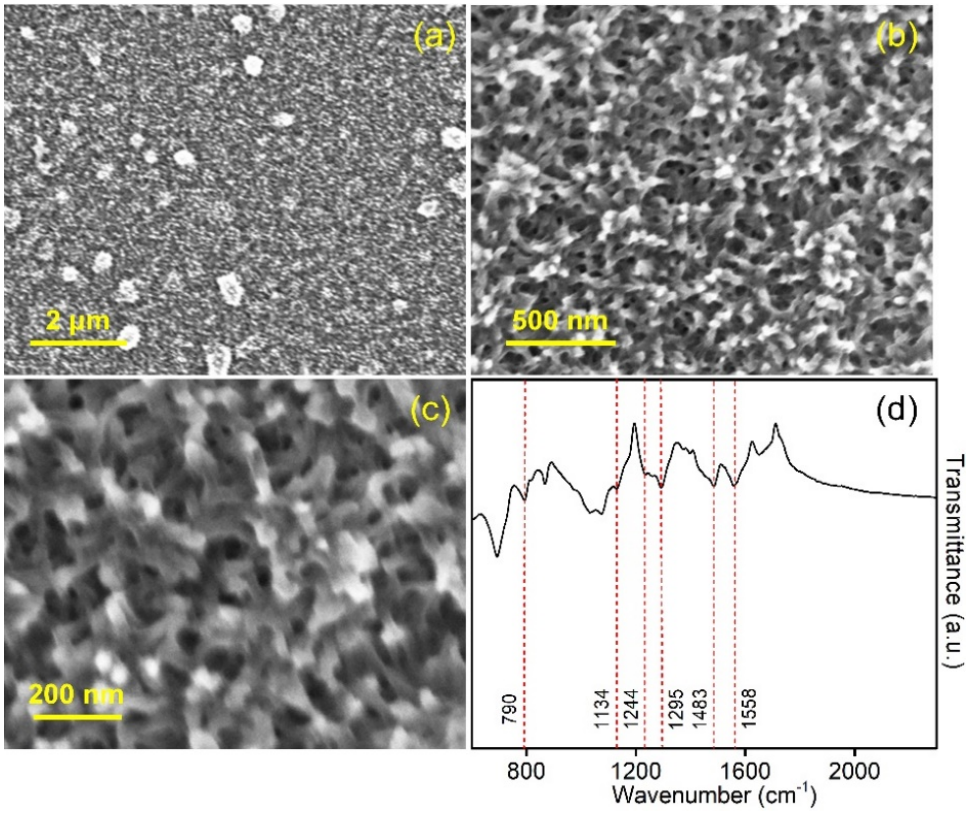

Figure S11: (a)-(c) FESEM images and (d) ATR-FTIR data of as-deposited PANI film

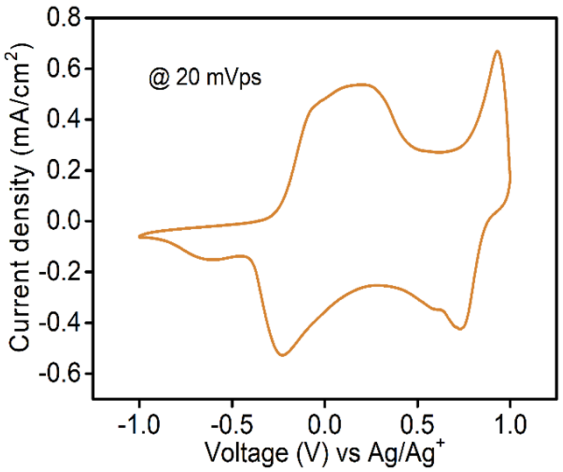

Figure S12: CV of PANI film in three-electrode set-up at 20 mVps scan rate in 1 M $LiClO_4$/PC electrolyte

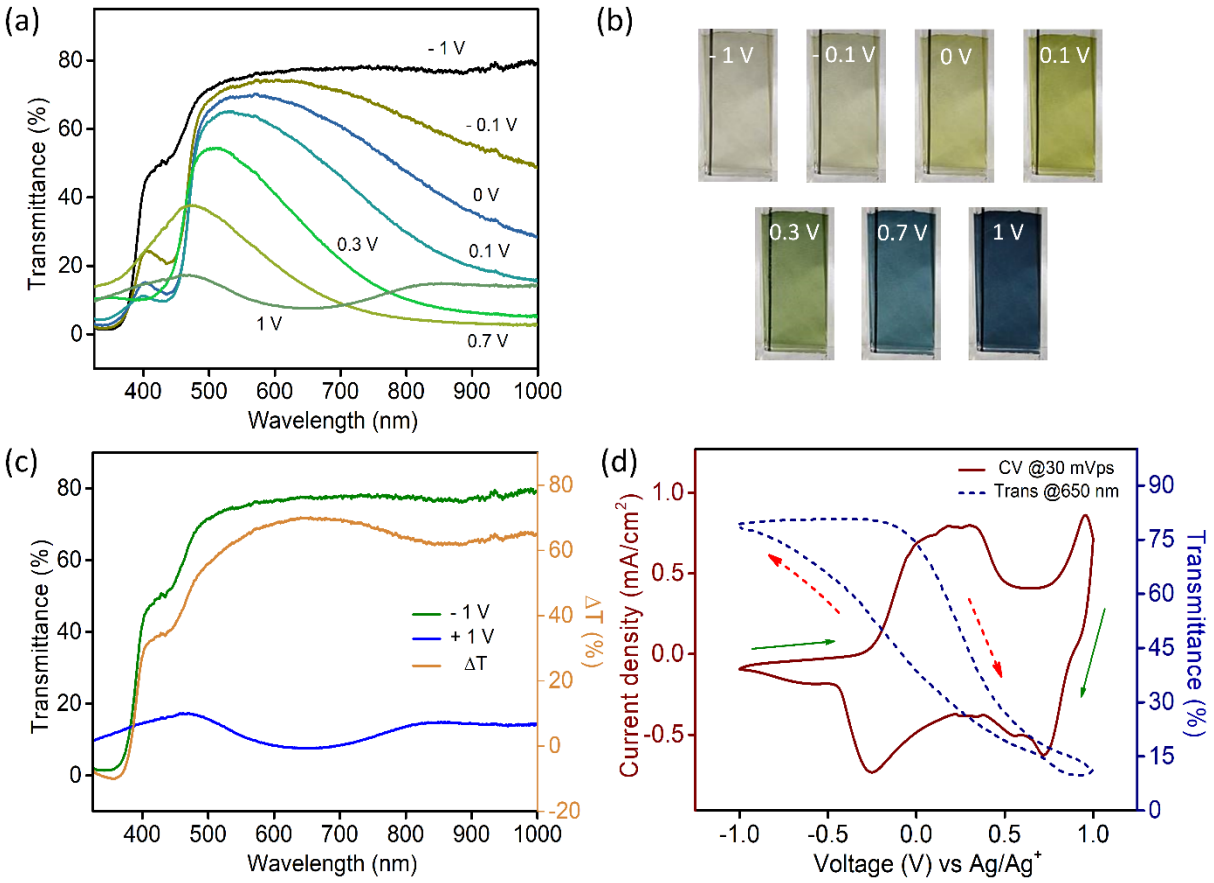

Figure S13: (a) Transmission spectra and (b) digital photographs of PANI electrodes at different applied biases, (c) Transmission data at +1 V and -1 V along with the optical modulation spectra (orange curve); (d) CV data of PANI film (wine curve) at 50 mV/s scan rate as well as the in-situ change in transmission at 650 nm (blue dotted line).

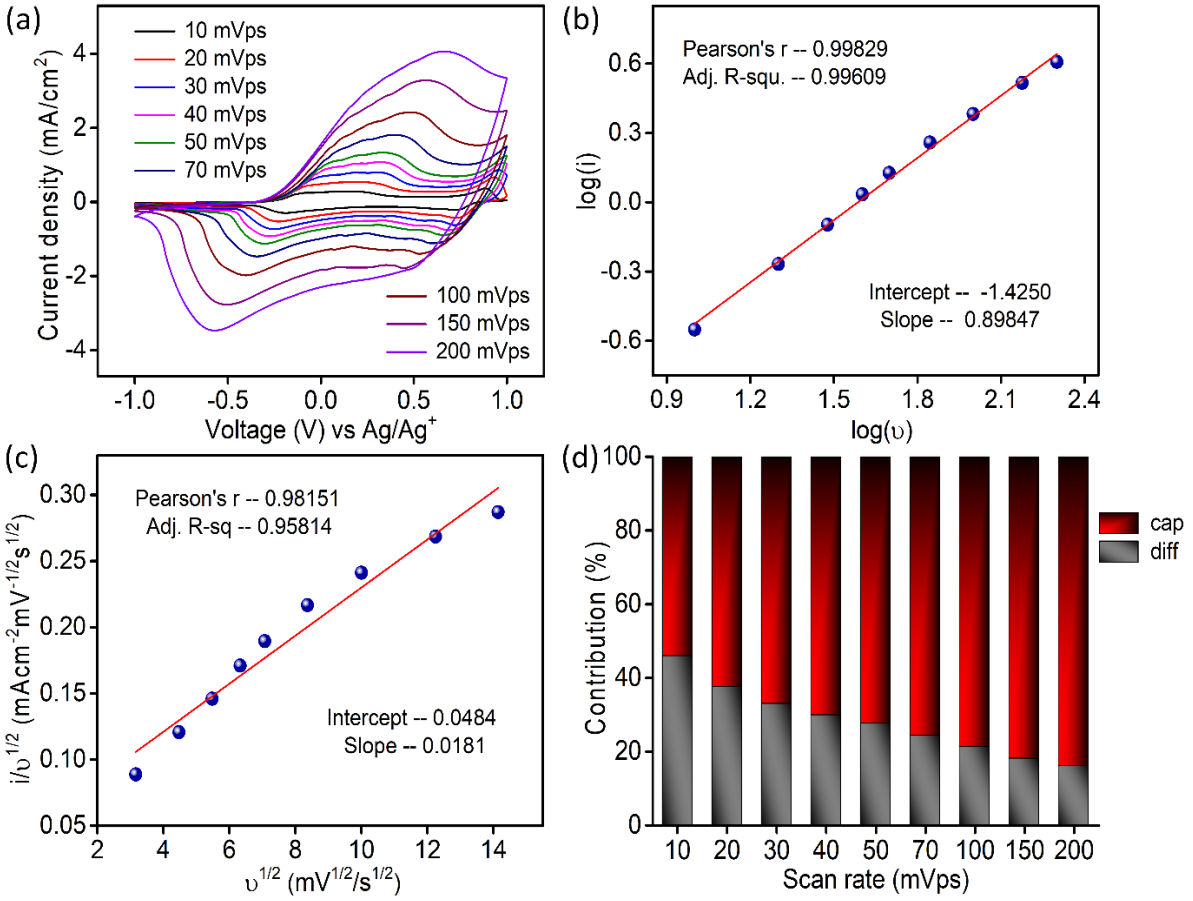

Figure S14: (a) Scan rate dependent CV data for PANI electrode, (b) log(i) vs log(υ) plot, (c) $i/\upsilon^{1/2}$ vs $\upsilon^{1/2}$ plot and (d) deconvoluting current contributions with scan rate

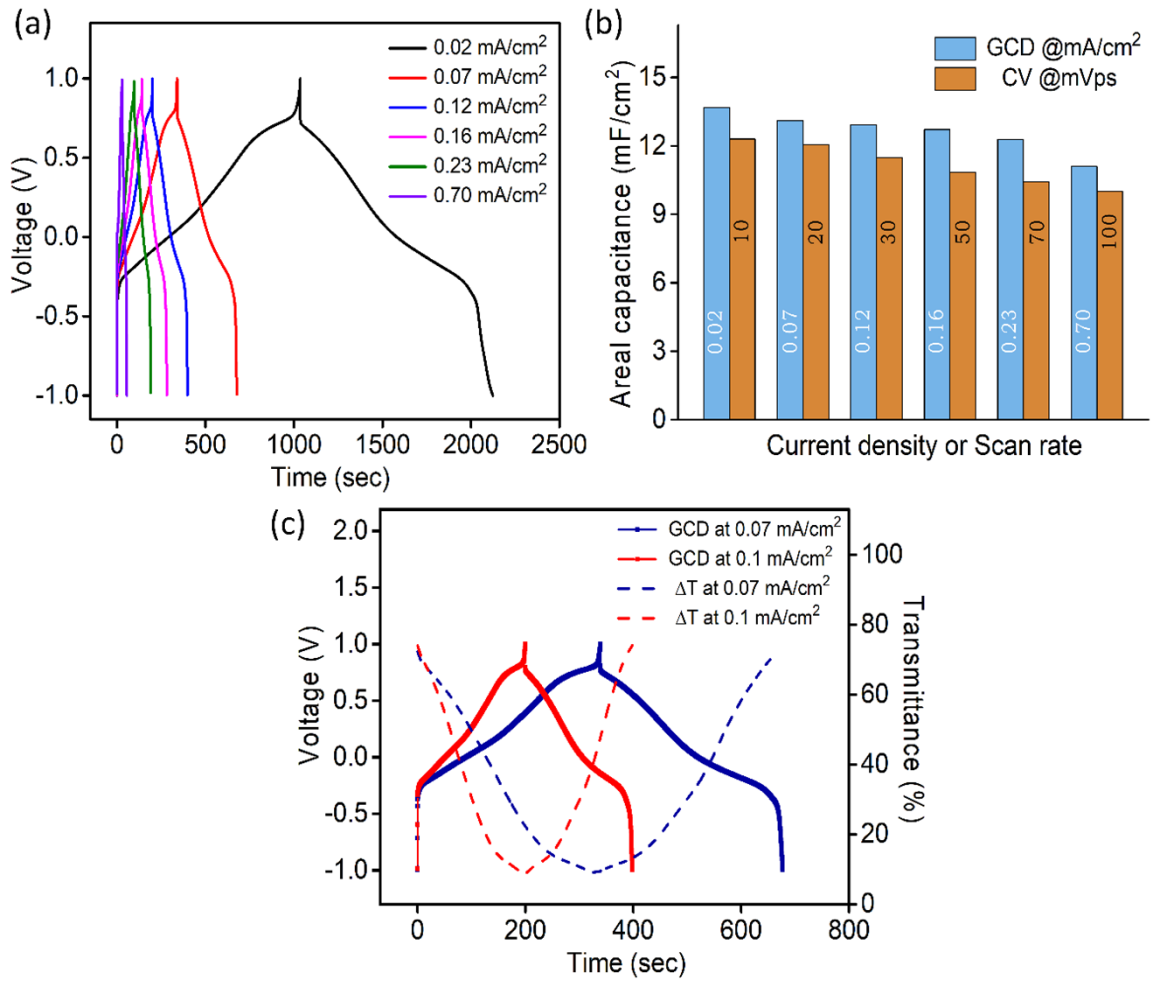

Figure S15: (a) GCD curves at different current densities; (b) comparison of areal specific capacitance values obtained from CV and GCD data; (c) in-situ change in transmittance at 650 nm synced with GCD curves at different current densities.

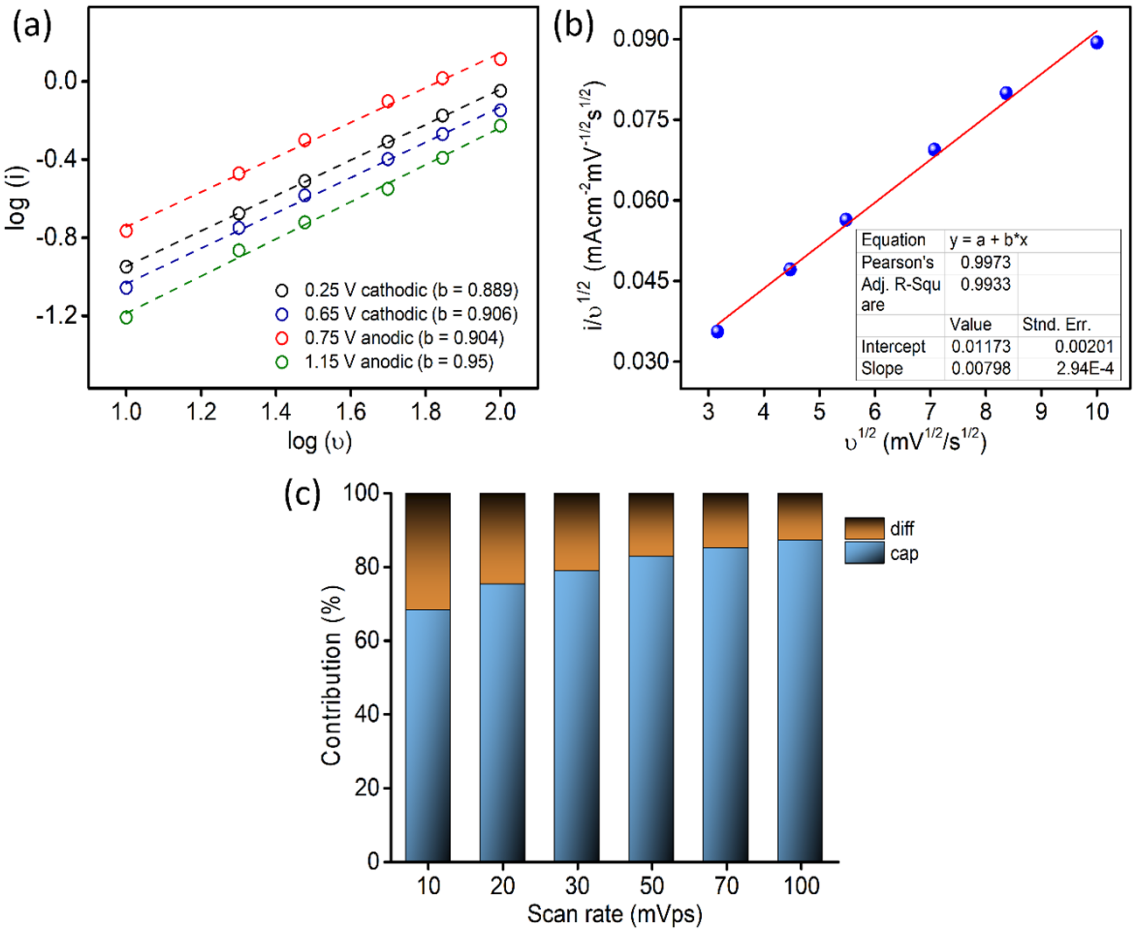

Figure S16: (a) log(i) vs log(υ) plot for ASC system at different voltages, (b) $i/\upsilon^{1/2}$ vs $\upsilon^{1/2}$ graph, (c) separating the current contributions at different scan rates

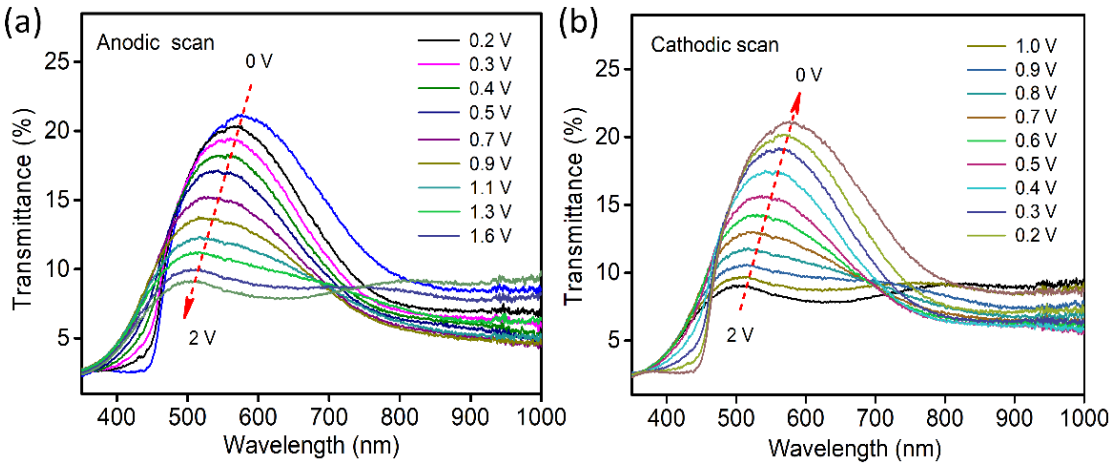

Figure S17: Gradual change in transmission spectra of MECASC during (a) anodic and (b) cathodic scan

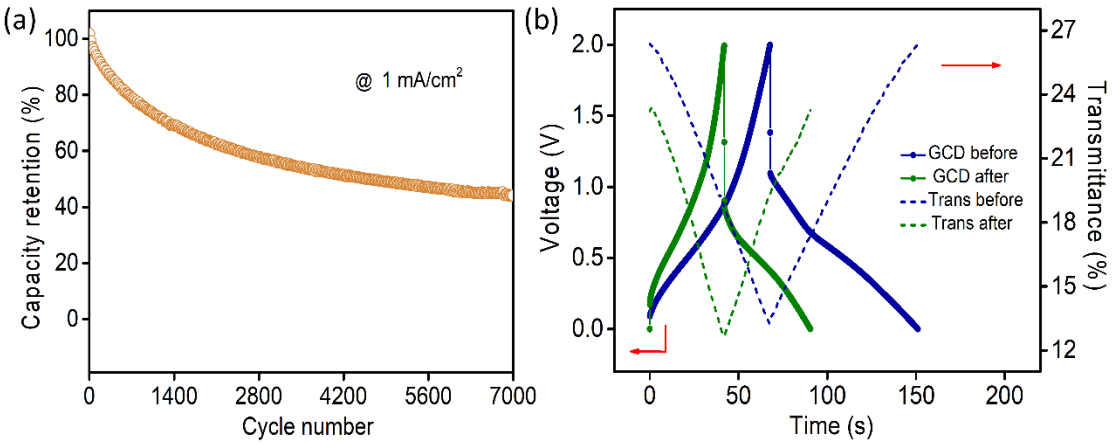

Figure S18: (a) Cycling performance of MECASC up to 7000 cycles; (b) GCD profiles of the system at 0.12 mA/cm^2 and dynamic in-situ transmission modulations at 580 nm before and after cycling

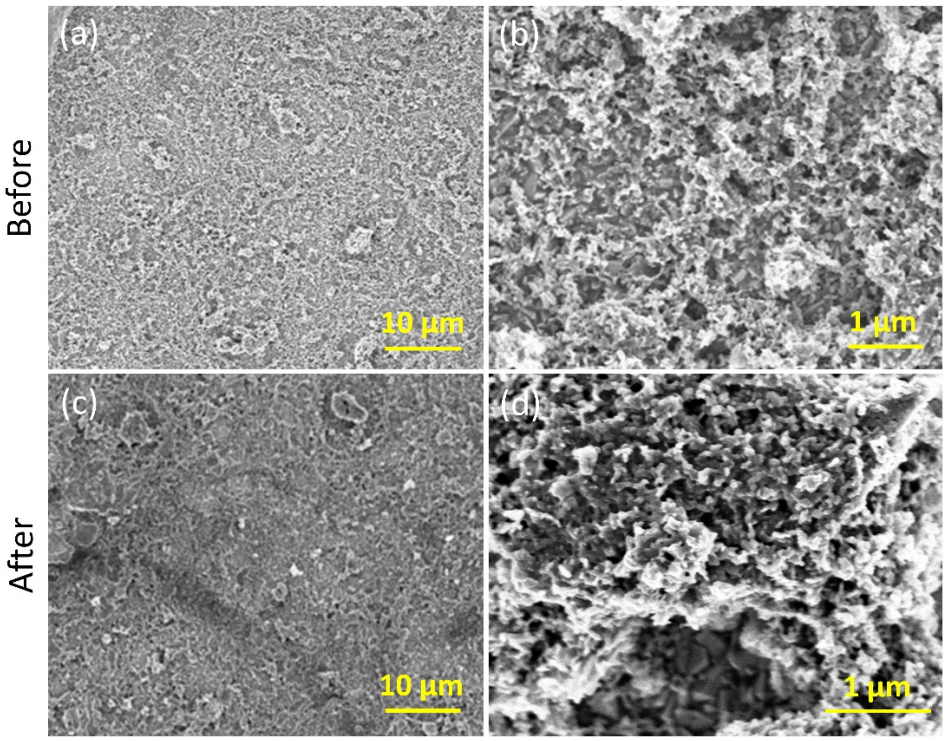

Figure S19: Morphology of V_2O_5 films before (a)-(b) and after (c)-(d) cycling in 2-electrode system at different magnifications

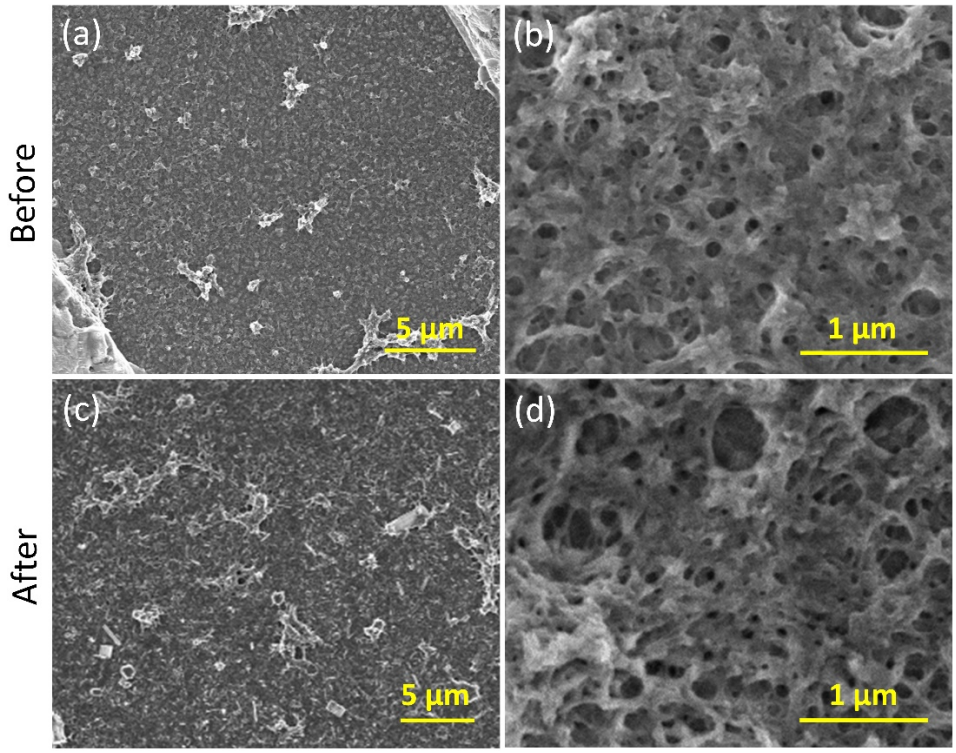

Figure S20: Morphology of PANI films before (a)-(b) and after (c)-(d) cycling in 2-electrode system at different magnifications